Original scientific paper
https://doi.org/10.33180/InfMIDEM2024.207

Informacije MIDEM
Journal of Microelectronics,
Electronic Components and Materials
Vol. 54, No. 2(2024), 149 – 161

Empirical Light-soaking and Relaxation Model of Perovskite Solar Cells in an Indoor Environment

Matija Pirc

Laboratory of Photovoltaics and Optoelectronics, University of Ljubljana, Faculty of Electrical Engineering, Ljubljana, Slovenia

Abstract: Perovskite Solar Cell (PSC) technology is approaching the level of maturity required for some niche applications, primarily in indoor environments. However, their metastability, expressed in the form of the light-soaking effect (LSE), makes it difficult to accurately estimate their expected real-life performance. This work demonstrates a new approach to LSE modelling, which can be used to determine the performance parameters of the PSC based on the history of its irradiance. The model was developed and tested on PSC performance data recorded during one month of operation in a realistic uncontrolled indoor environment, two days of which were used for the tuning of the model and the rest for its verification. The presented model was compared to two static one-diode models, which do not account for the LSE. The energy yield prediction error of the new model was only -0.72 %, the error of the static model based on low-light measurements was +6.96 %, and the error of the static model based on measurements under standard test conditions (STC) was +7.76 %. EY prediction of the low-light static model can however be arbitrarily improved by cherry picking the I-V curve on which to base the model, once the expected result is known. A more meaningful measure of model performance is the mean absolute error (MAE) of the predicted power at the maximum power point PMPP. The MAE of PMPP predicted by the new model was 16.7% lower than that of the low-light static model and 17.1 % lower than that of the STC static model.

Keywords: perovskite solar cells; light-soaking; indoor photovoltaics; I-V curve; energy yield

Empirični model svetlobnega prežemanja in relaksacije perovskitnih sončnih celic v notranjem okolju

Izvleček: Tehnologija perovskitnih sončnih celic (PSC) se približuje stopnji zrelosti, ki je potrebna za vstop na trg nekaterih nišnih aplikacij, predvsem v notranjem okolju. Zaradi njihove metastabilnosti, ki se izraža v obliki učinka svetlobnega prežemanja (ang. Light-soaking Effect - LSE), težko natančno ocenimo njihovo pričakovano učinkovitost v realnem okolju. To delo prikazuje nov način modeliranja LSE, ki omogoča napovedovanje delovanja PSC na podlagi zgodovine obsevanosti. Model je bil razvit in preizkušen na enomesečnih meritvah delovanja PSC v realnih nenadzorovanih notranjih pogojih delovanja. Podatki dveh dni so bili uporabljeni za umerjanje modela, preostali podatki pa za preverjanje njegovega delovanja. Predstavljeni model smo primerjali z dvema statičnima enodiodnima modeloma, ki ne upoštevata LSE. Napaka napovedi energijskega izplena novega modela je bila le -0,72 %, medtem ko je napaka statičnega enodiodnega modela, osnovanega na meritvah pri nizki osvetljenosti, znašala +6,96 % in napaka statičnega enodiodnega modela, osnovanega na meritvah pod standardnimi testnimi pogoji (ang. Standard Test Conditions - STC), znašala +7,76 %. Napoved energijskega izplena statičnega modela osnovanega na meritvah pri nizki osvetljenosti, je mogoče pri znanem želenem rezultatu skoraj poljubno izboljšati z izbiro krivulje I-U, na kateri ta model temelji, zato napaka energijskega izplena ni najboljše merilo uspešnosti modela. Boljše merilo je srednja absolutna vrednost napake (ang. Mean Absolute Error - MAE) napovedane moči v točki največje moči PMPP. MAE napovedane PMPP novega modela je bila za 16,7 % manjša od MAE napovedi statičnega modela, osnovanega na meritvah pri nizki osvetljenosti in 17,1 % manjša od MAE napovedi statičnega modela, osnovanega na STC meritvah.

Ključne besede: perovskitne sončne celice, svetlobno prežemanje, notranja fotovoltaika, I-U karakteristika, energijski izplen

** Corresponding Author's e-mail: matija.pirc@fe.uni-lj.si*

How to cite:
M. Pirc, "Empirical Light-soaking and Relaxation Model of Perovskite Solar Cells in an Indoor Environment", Inf. Midem-J. Microelectron. Electron. Compon. Mater., Vol. 54, No. 2(2024), pp. 149–161

1 Introduction

In the field of photovoltaics (PV) perovskite solar cells (PSC) have received a lot of attention during the last decade due to their high power conversion efficiency (PCE) potential [1], [2] and simple and low cost production process [3]–[5]. Despite their great advantages, they also have a few weaknesses hindering their widespread adoption, namely the use of toxic materials like lead [6]–[8] and their less than desirable long-term stability [9], [10]. However, intense research efforts are also improving these areas to the point that commercial applications are becoming feasible [11]. One of the niches the first commercial PSCs will most likely flourish in is indoor PV [12], [13], due to the mild operating environment, and their high and tunable bandgap energy [14]–[16], which makes them particularly suitable for use with artificial light sources that emit light in the human visible light spectrum by design. At the same time, a vast opportunity for indoor PV is opening with the rapid expansion of the Internet of Things (IoT) market [17] and PSCs could be the perfect solution.

For any PV use case an estimation of power capacity and expected energy yield (EY) is required. The estimation process can be as simple as taking the average irradiation and nominal solar cell efficiency to get a rough estimation of expected EY or an in-depth analysis taking into account measured device characteristics, temperature dependence, angular irradiance distribution, spectra, etc. [18]–[22]. Such analysis is not only useful for adequate sizing of PV installations or PV devices, but also for optimizing the structure of PV devices[18], [21], real-time monitoring and early fault detection by comparing the predicted and real performance of an installation, as well as gaining deeper insights into the operation of solar cells.

Although methodologies for predicting solar cell performance and calculating EY have evolved significantly and are capable of remarkable accuracy in the case of established technologies like silicon solar cells, PSCs are still a challenge due to their short-term instability, widely known as the light-soaking effect (LSE). A simple approach to sidestepping the challenges of the LSE in outdoor environments is to use the performance characteristics of a fully light-soaked PSC throughout the whole day [22]. This method is quite accurate for outside environments on bright sunny days when the LSE rapidly reaches saturation. However, in indoor environments, or even outdoors on particularly cloudy or foggy days, the LSE is much slower due to lower irradiance and may not reach saturation at all, yet still significantly affects the performance [23], [24]. In these cases, a method for predicting the state of the LSE of a PSC based on the history of its irradiance could significantly improve the accuracy of the PSC energy yield calculations.

Many mechanisms contribute to the LSE, e.g. light induced ion migration, trap defect passivation, charge carrier accumulation, lattice expansion, etc. [25]–[28]. The bulk of the research of the LSE focuses on understanding the mechanisms behind it and the models developed are quite involved and usually require in-depth knowledge of the specific PSC. For the purpose of long-term performance predictions, these models are often computationally too intensive and require device parameters which are challenging to acquire. Long-term performance modelling generally requires different, high-level models, which are comparatively easy to tune and use on large data sets of environmental parameters.

In this contribution, we present an empirical model of the LSE which was developed by analyzing recorded data of PSC performance in a realistic, uncontrolled indoor environment. The model can be tuned on a few days' worth of measured data and then used to predict the *I-V* curves of the PSC based on the history of its irradiance for any point in time. We also discus the shortcomings of the model and explore the possibilities of further research and improvements.

2 Materials and methods

2.1 Measurement Setup

PSC performance and environmental parameters were monitored and logged by an in-house designed Indoor Monitoring System which is thoroughly described in [24], therefore only the relevant details will be repeated here. The system maintains four solar cells at the MPP, and logs the average values of their performance, irradiance, temperature and humidity every 5 minutes. Additionally, *I-V* scans of all the cells are performed every half an hour. *I-V* scans are performed in voltage steps of approximately 20 mV every 60 ms, starting at V_{OC} , sweeping down to 0 and then back up to V_{OC} . During each step, the irradiance is measured and stored with the *I-V* data to facilitate subsequent detection of unsuitable lighting conditions, e.g. sudden changes in the irradiance during an *I-V* scan.

The system was designed to mimic a realistic indoor PV powered device between *I-V* scans, which would shut down MPP tracking when the energy cost of MPP tracking would exceed energy gains. Therefore, when the current of the PSC falls below 30 µA, MPP tracking and energy harvesting is suspended.

The monitoring system was located on a shelf approximately at the center of the Laboratory of Photovoltaics and Optoelectronic office 1 (LPVO-1) in Ljubljana, Slovenia, with windows facing north-north-west (336°). This means that direct sunlight is possible only for a few minutes in the evenings from about a month before to about a month after the summer solstice, which was not the case within the timespan of the measurements used here.

Irradiance was measured with a silicone photodiode SFH2440L with an IR-cut filter, to adjust the spectral response of the photodiode to be more similar to the spectral response of the PSC. Unfortunately, the difference between both spectral responses is still quite large and since the spectrum of light changes considerably when the ratio of natural and artificial lighting changes, the irradiance measurement accuracy leaves something to be desired. Although the accuracy is sufficient for the LSE modelling and performance prediction, PCE calculations based on these measurements are not recommended.

2.2 Perovskite solar cell

The structure of the PSC was glass | ITO | MeO-2PACz | perovskite | C_{60} | SnO_2 | Cu in a p-i-n architecture, where the MeO-2PACz monolayer (2-(3,6-Dimethoxy-9H-carbazol-9-yl)ethyl)phosphonic acid) is a hole transport layer (HTL), and the C_{60} and SnO_2 layers are electron transport layers (ETL). The perovskite absorber is a formamidinium-caesium (FACs) double cation perovskite absorber with the chemical formula $FA_{0.83}Cs_{0.17}Pb(I_{0.83}Br_{0.17})_3$. The back and front contacts are connected with 2 self-adhesive copper stripes. The device is sealed between 2 sheets of glass with two-component 5-minute epoxy. The area of the PSC is 1.06 cm^2 and under standard test conditions (STC) the short-circuit current density is 22.3 mA/cm^2, open-circuit voltage 1.13 V, fill factor 78.6 % and PCE 19.9 %. The *J-V* curve under STC and the external quantum efficiency (EQE) of the PSC, along with the EQE of the photodiode for measuring irradiance are shown in Figs. 1 and 2, respectively.

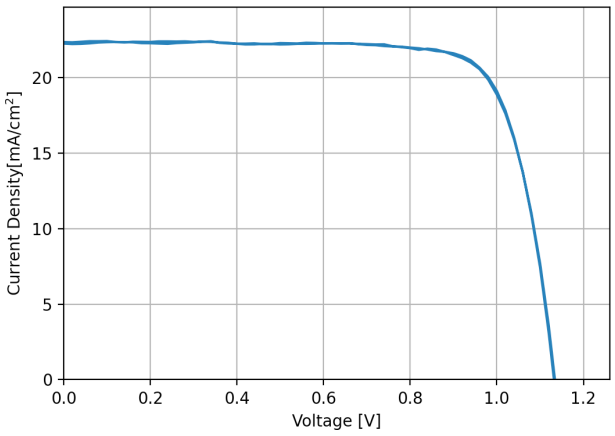

Figure 1: J-V of the PSC under STC

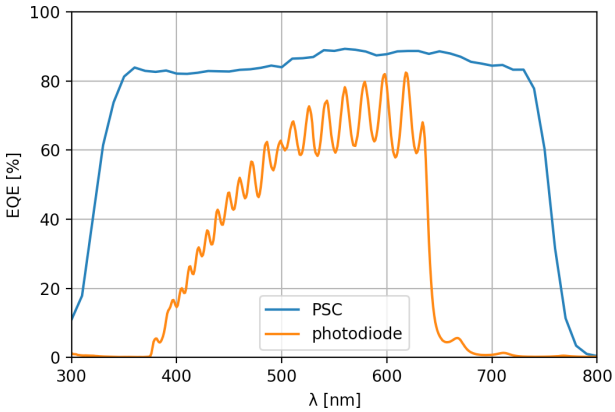

Figure 2: Spectral response of the PSC and photodiode with IR-cut filter for measuring irradiance.

2.3 Data preparation

Because the measurements were performed in an uncontrolled environment, not all the measurements were valid, e.g. when the irradiance was changing too much during the *I-V* scan. To filter out these scans, the standard deviation of the irradiance during each *I-V* scan was calculated and all *I-V* scans with a standard deviation of irradiance larger than 1 % of the average irradiance or larger than 0.005 W/m^2 were ignored. *I-V* scans with an average irradiance lower than 0.15 W/m2 were also ignored, because the current measurement noise becomes too prevalent at such low irradiance. For easier comparisons with other studies all cell parameters and measurements were normalized to the area of 1 cm^2.

3 The Light-soaking Model

The effect of Light-soaking can be readily discerned by observing the *J-V* scans taken throughout a typical day. Fig. 3 shows the *J-V* scans recorded on August 1, 2022 progressing from light to dark color from the morning to the evening. The LSE is most apparent when comparing the *J-V* scans taken very early in the morning and very late in the evening. When the two marked scans were acquired, the irradiance was very similar (0.80 and 0.76 W/m2, respectively), yet the V_{OC} was 90 mV higher in the evening (15 %), even though the irradiance was slightly lower.

Even though the LSE is most evident in increased V_{OC}, the V_{OC} has a very strong dependence on the irradiance

G, which makes it impossible to determine the size of the LSE from the V_{OC} alone.

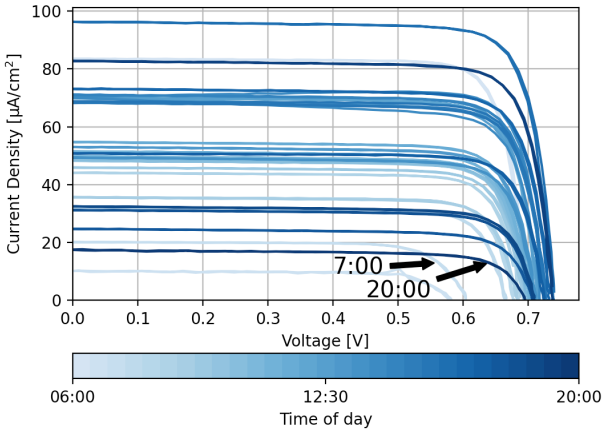

Figure 3: *J-V* scans of the PSC recorded on August 1, 2022. Line color hue indicates the time of the scan – from bright in the morning to dark in the evening. The two marked lines show the LSE most prominently.

3.1 One-diode Model Parameters

Power and EY calculations are possible as soon as the *JV* curves for each point in time are determined. Solar cell *J-V* curves are often modelled by a one- or two-diode model. If the parameters of the model can be determined, all other calculations can be performed as well. To see if the parameters of such a model could be used to predict the influence of the LSE, a mass fit on all the *J-V* scans of the PSC acquired in august 2022 was performed using the 2/3 Diode Fit program [29]. With some experimentation we determined that a one-diode model is sufficient to achieve a very good fit for all the *J-V* scans and with the low irradiance in the indoor environment and therefore small currents, even the series resistance of the one-diode model can be safely disregarded. The one-diode model used in the study is shown in Fig. 4 and it is described by equation (1)

$$J = J_{PH} - J_S\left(\exp\left(\frac{V}{nkT/q}\right) - 1\right) - \frac{V}{R_P} \qquad (1)$$

where J_{PH} is photo-current density, J_S saturation current density of the diode, *n* ideality factor, *k* Boltzmann constant, *T* temperature, *q* electron charge, R_p shunt resistance and *V* voltage of the solar cell.

The photo-current density J_{PH}, which, in the case of zero series resistance, is equal to the short-circuit current density J_{SC}, is expected to be directly proportional to the irradiance *G*. This was confirmed by Fig. 5, which shows that measurements exhibit linear dependence

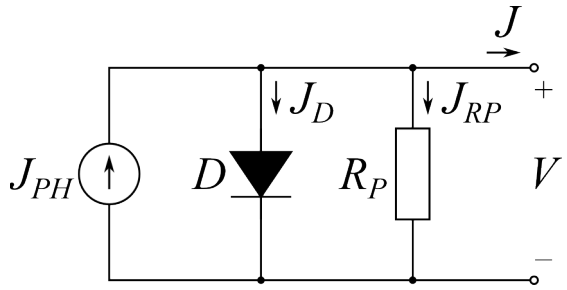

Figure 4: One-diode model used to model the PSC.

on irradiance with deviations of only a few percent, except for a few outliers most likely resulting from local shading.

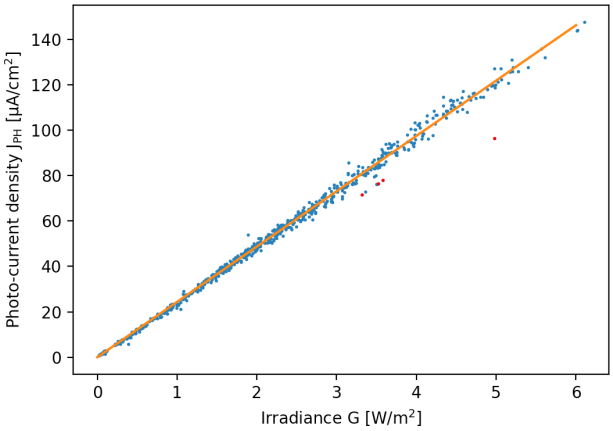

Figure 5: Short-circuit current density J_{SC} of all *J-V* scans vs. irradiance *G*(blue dots) and a linear fit to the data (orange line). The few red dots are considered to be outliers. The R^2 score of the fit without the outliers is 0.996.

Plotting the time evolution of the fitted parameters of the one-diode model unveils a weak correlation be-

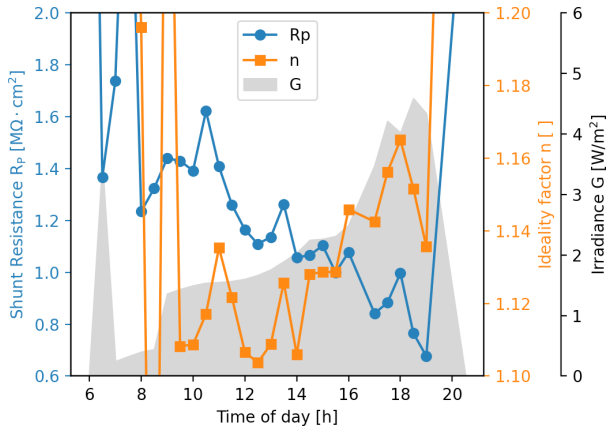

Figure 6: Time evolution of the ideality factor *n* (orange squares) and parallel resistance R_p normalized to 1 cm² (blue circles) on August 5, 2022. The gray fill shows irradiance.

tween the ideality factor *n* and the irradiance *G*, as well as an inverse correlation between the parallel resistance R_P and the irradiance *G* throughout most of the day. Fig. 6 shows *n*, R_P and *G* on August 5, 2022. This date was selected because irradiance more or less steadily rises during the day, making it easier to perceive the observed correlations.

Saturation current density J_S on the other hand does not seem to have an obvious direct correlation to irradiance. Therefore Fig. 7 shows its time evolution for all days in August. On most days (but not all) the J_S starts quite high, drops by 2 or 3 orders of magnitude in the first 2 hours, and after that more or less steadily falls until the evening.

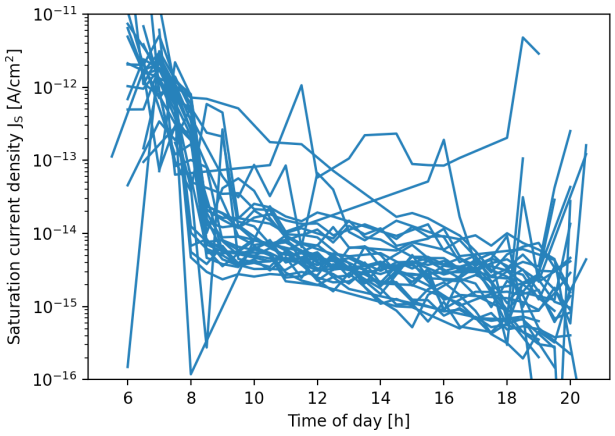

Figure 7: Time evolution of the saturation current density J_S throughout every day of August 2022.

The correlations of *n* and R_P to *G* are discernible between approximately 9:00 or 10:00 in the morning and 18:00 or 19:00 in the evening. Before and after that the correlations don't seem to hold or they are simply lost in the noise. When irradiance is low, the noise in the measurements makes for a very undefined fit, which can result in very large and unrealistic swings in parameter values.

To verify the observed correlations, we plotted the one-diode parameters of all *J-V* curves as a function of irradiance, shown in Figs. 8 through 10. The majority of values of the ideality factor *n* fall within a narrow range between 1.1 and 1.2 with some outliers, especially at lower irradiance values, falling outside this range. Values that do fall within this range seem to exhibit a slight linear dependence on irradiance, confirming the previous observation. It is likely that some of the outliers are not just the result of ambiguity when fitting the one-diode model to noisy data, but instead the ideality factor may also depend on the state of light-soaking. However, at this stage we are not yet sure if that is really the case, and for now we consider data points that deviate enough from the main linear trend as outliers. The linear fit

$$n = n_0 + k_n G \tag{2}$$

depicted by the orange line in Fig. 8, where *G* is irradiance, the intercept n_0 is 1.094 and the linear coefficient k_n is 0.015 m²/W, was performed using the RANSAC linear regression method (RANdom SAmple Consensus) from the python package Scikit-learn [30] with the residual threshold value of 0.05. The red dots in Fig. 8 are the ideality factor values which the RANSAC algorithm marked as outliers. Due to the intrinsic randomness of the RANSAC algorithm, the fit is slightly different for each run. The R^2 score of the fit without outliers varies between 0.5 to 0.7 from run to run.

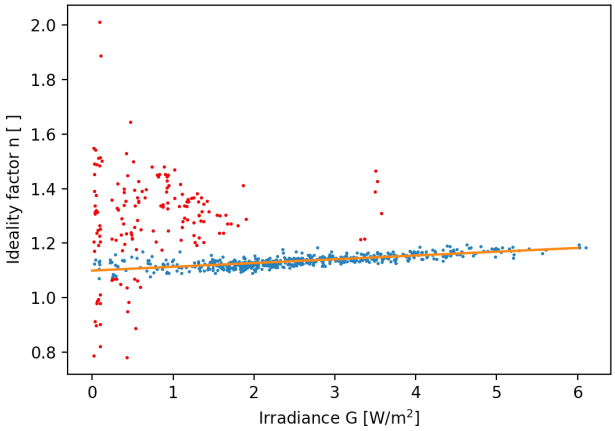

Figure 8: Ideality factors *n* of all the fits to *J-V* curves vs irradiance *G* (dots) and a linear fit to the data (orange line). The red dots are outliers as determined by the RANSAC fit method. The R^2 score of the fit without the outliers averages around 0.6.

Parallel resistance values (Fig. 9) mostly fall between 0.8 and 3 MΩ·cm². Values larger than that have almost no influence on the *J-V* curve (smaller than the measurement accuracy), and are therefore just an artifact of the one-diode model fitting process. The datapoints give an impression of negative exponential relation to irradiance, which is similar to the inverse correlation observed in the time evolution of parallel resistance and irradiance shown in Fig. 6. We modelled the relation between parallel resistance RP and irradiance G with the equation (3)

$$R_P = R_{PMIN} + R_{PE} \exp\left(-\frac{G}{G_K}\right) \tag{3}$$

depicted by the orange line in Fig. 9, where *G* is irradiance, R_{PMIN} is 0.784 MΩ·cm², R_{PE} is 1.390 MΩ·cm² and G_K is 1.440 W/m². The fit was acquired using a similar

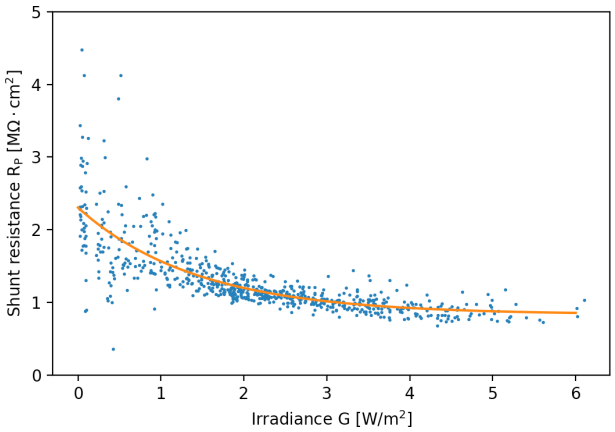

Figure 9: Parallel resistance R_p of all the fits to *J-V* curves vs irradiance *G* (blue dots) and an exponential fit to the data (orange line). The R^2 score of the fit without outliers is 0.637.

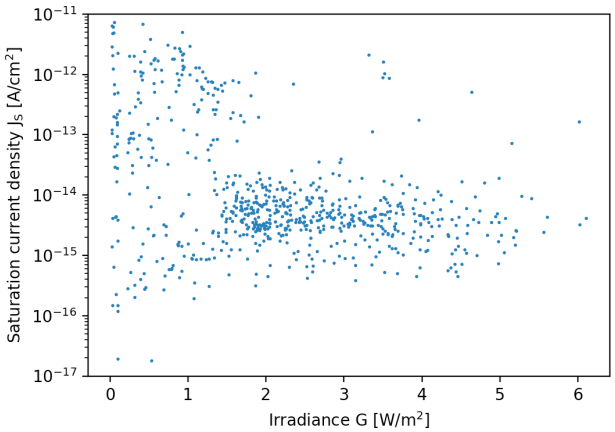

Figure 10: Saturation current J_s of all the fits to *J-V* curves vs irradiance *G*.

approach to the RANSAC linear regression method, but using our own code built on top of the python lmfit package, since the Scikit-learn package does not have a built-in function for RANSAC exponential regression. In the case of parallel resistance, the outliers are much more obvious (out of range of Fig. 9) than in the case of the ideality factor, therefore more or less the same datapoints are marked as outliers in each run and the results of the fit are much more consistent from run to run. The R^2 score of the fit without outliers is 0.637.

Saturation current densities resulting from the fittings of the data to the one-diode model, shown in Fig. 10, span a large range of values and do not show a direct correlation to irradiance as already expected based on Fig. 7. Therefore, we assume that the greater part of the LSE is encompassed within this parameter.

For additional context, the one-diode parameters of the same PSC have been extracted from the *I-V* curve measured after the PSC was fully light-soaked under STC. In this case the saturation current density J_S is $1.1 \cdot 10^{-10}$ A/cm², the ideality factor *n* is 2.31, and parallel resistance R_p is infinite (any value above 10 kΩ gives good fit results). On the other hand, the model does require a series resistance of 1.15 Ω. The measured short-circuit current density is 22.3 mA/cm², which is 13.5 % lower than would be expected based on the photocurrent dependence on irradiance shown in Fig. 5. The ideality factor is considerably larger than in low light conditions, however, based on equation (2) it should be about 7 times larger still, showing that the linear fit is only valid within the range of low irradiances.

3.2 Linking one-diode model parameters to a single observable of the LSE

The challenge of predicting the size of the saturation current lies in its very large range of possible values as well as in its close connection to the ideality factor n. A small change in the ideality factor n, can be compensated with quite a large change in the saturation current density to achieve an almost identical J-V scan fit, as shown in Fig. 11. The two fits shown represent the measured data practically equally well, but the saturation current density of the second fit is approximately 5 times larger than that of the first fit while the difference in the ideality factor is less than 10 %. The parallel resistance is the same in both cases. This means that predicting the value of the saturation current independently from the ideality factor would not be the most reliable way of predicting the size of the LSE. Therefore, a more robust parameter, combining the saturation current density with other parameters, would be a better option for predicting the LSE.

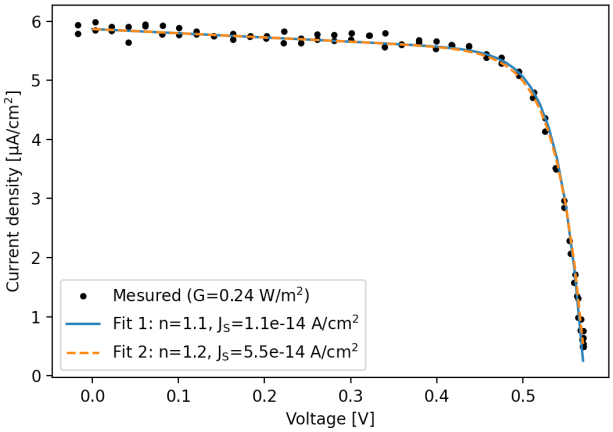

Figure 11: Demonstration of strong dependence of the J_S parameter on the *n* parameter of the one-diode model – under 10 % change in *n* requires 500 % change in J_S, to get an almost identical fit within the measured range of data.

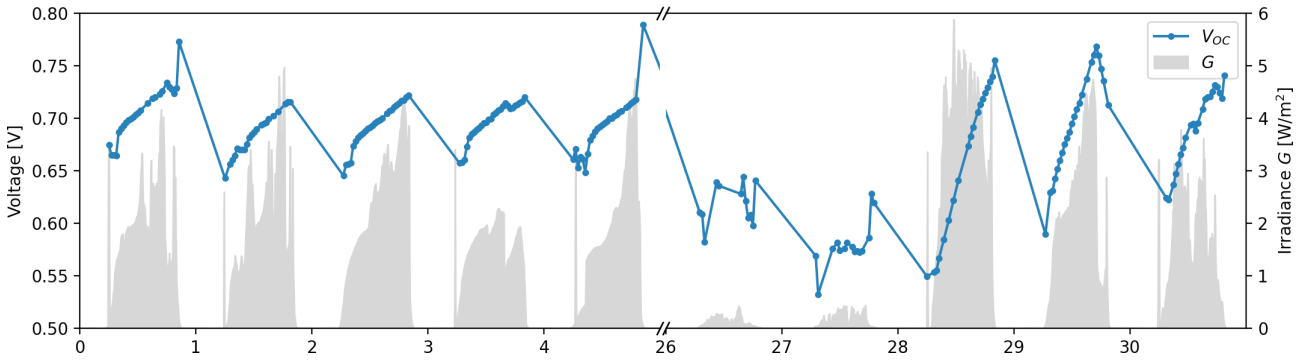

Figure 12: Time evolution of V_{OC} at a pre-selected photo-current density of 73.3 µA/cm², equivalent to irradiance of 3 W/m², during the first 5 and last 5 days of August.

Open-circuit voltage is the most obvious parameter where the effects of light-soaking are evident. However, as already mentioned, it also strongly depends on the photocurrent, which in turn depends on the irradiance. The effect of light-soaking on the V_{OC} could be isolated from the direct effect of the irradiance if the *I-V* curves were always measured at the same irradiance. Although this was not possible within the experiment, such a measurement should only marginally affect the shape of the curve through minor changes to the ideality factor and the parallel resistance according to (2) and (3), provided the scan time at a different irradiance was short enough not to meaningfully change the amount of light-soaking. On the other hand, once a one-diode model fit is obtained, a V_{OC} at a pre-selected photo-current can be easily calculated with reasonable accuracy. Fig. 12 shows the time evolution of the calculated V_{OC} at a pre-selected photo-current density of 73.3 µA/cm², which corresponds to 3 W/m² irradiance – approximately half of the maximum irradiance measured in August.

The time evolution of the V_{OC} at the pre-selected current indicates that the LSE more or less steadily increases throughout most days, with quite a weak dependence on the irradiance and only shows a decrease when the irradiance drops very drastically. Combining these observations with the observed speed with which the LSE increases under STC or in an outdoor environment compared to the indoor environment, leads us to believe that the speed of the LSE, or at least this parameter which indicates the state of the LSE, is proportional to the logarithm of the irradiance.

3.3 Discrete linear time-invariant system for LSE dependent VOC prediction

Previous studies [26], [27] have shown that at a constant irradiance, the V_{OC} of a PSC follows an increasing exponential decay form with an offset V_{OCMIN} (4), reminiscent of the voltage of a capacitor while charging to a fixed voltage through a resistor, if the offset is ignored.

$$V_{OC}(t) = V_{OCMIN} + V_{OCLS}\left(1 - \exp\left(-\frac{t}{\tau}\right)\right) \tag{4}$$

The time evolution of the V_{OC} in Fig. 12 looks like it could fit the same increasing exponential decay form, but with quite a long time constant. In light of this, we sought to model the LSE with a linear time-invariant (LTI) system, which takes a logarithm of the time resolved irradiance as an input and outputs the time resolved V_{OC} at a pre-selected current density. The predicted V_{OC} calculated for each point in time can then be used together with the ideality factor *n* and parallel resistance R_P calculated from the irradiance using (2) and (3) to determine the saturation current density J_S.

The step response of the system shown in (4) has an offset V_{OCMIN}, which has to be treated separately since a system with an offset does not satisfy the homogeneity condition for linearity and is therefore not an LTI system. The step response of the linear part of the system is therefore

$$V_{OC}(t) = V_{OCLS}\left(1 - \exp\left(-\frac{t}{\tau}\right)\right) \tag{5}$$

where τ is the time constant of the LSE and V_{OCLS} is the size of the input step function determined by the irradiance and represents the final increase of the V_{OC} due to the LSE. The $V_{OC}(t)$ is assumed to be 0 for $t < 0$, but is not denoted within the equation by multiplication of the right-hand side with a unity step function for clarity's sake, as will be the case henceforth.

The LTI system could be modelled by a resistor-capacitor (RC) electrical circuit, and its response calculated by any electrical circuit simulator. However, since all the

measured data, including the irradiance, which will be the input to the system, is sampled at discrete points in time, it is more convenient to construct and run a discrete-time LTI system with an equivalent response. To do that, we first rewrite (5) as a unit step response $g(t)$ and derive the system's impulse response $h(t)$

$$g(t) = 1 - \exp\left(-\frac{t}{\tau}\right) \tag{6}$$

$$h(t) = \frac{\mathrm{d}g(t)}{\mathrm{d}t} = \frac{1}{\tau}\exp\left(-\frac{t}{\tau}\right) \tag{7}$$

Periodically sampling the impulse response with a sampling period of T_S, we get

$$h(nT_S) = \frac{1}{\tau}\exp\left(-\frac{nT_S}{\tau}\right) \tag{8}$$

which can be rewritten in its discrete-time form as

$$h[n] = K \cdot a^n \tag{9}$$

where K equals $1/\tau$ and a equals $\exp(-T_S/\tau)$.

The Z-transform of (9)

$$H(z) = K \cdot \frac{z}{z-a} \tag{10}$$

can be used to construct a difference equation of a discrete-time system

$$y[n] = K \cdot x[n] + a \cdot y[n-1] \tag{11}$$

where x[n] are the consecutive input values of the system (logarithm of the irradiance) and y[n] are the consecutive output values of the system (increase of the V_{OC} due to the LSE).

Before the logarithm function can be applied to the irradiance, the irradiance needs to be normalized to a reference value. We assume some minimal irradiance is required for the processes contributing to the LSE to start, although so far, we have not found any reports on the matter. Therefore, we define the logarithmic irradiance GL as

$$GL = \log_{10}\frac{G}{G_{MIN}} \tag{12}$$

The values of the irradiance G are also downward limited to G_{MIN} to avoid negative and complex values of GL, which can appear when negative values of irradiance are measured due to noise when the real irradiance is below the noise threshold of the instrument. The complete model for predicting the V_{OC} is described by Pseudo-code 1:

Pseudo-code 1: V_{OC} prediction model.

INPUT: vector G
OUTPUT: vector V_{OC}

$V_{OCLS}[0] = V_{OCLS0}$
for n = 1 to length(G)-1
$G_{LIM}[n] = \max(G[n], G_{MIN})$
$GL[n] = \log_{10}(G_{LIM}[n]/G_{MIN})$
$V_{OCLS}[n] = K \cdot GL[n] + a \cdot V_{OCLS}[n-1]$
$V_{OC}[n] = V_{OCMIN} + V_{OCLS}[n]$
end for

Before the model can be used for predicting the values of the V_{OC} at the pre-selected photo-current, the constants G_{MIN}, V_{OCLS0}, K, a, and V_{OCMIN} have to be tuned to the specific solar cell. This can be achieved by treating the constants as parameters of a model, and fitting the model to the known values of the V_{OC} at the specific times when it was measured. We used the data of the first 2 days to tune the model and the rest of the data to assess the performance of the model. The values of the constants after the tuning process are collected in Table 1.

Table 1: Tuned model parameters.

Parameter	Value
G_{MIN}	0.0001 W/m^2
V_{OCLS0}	0.303 V
V_{OCMIN}	0.425 V
K	2.949·10-4 V
a	0.99689

4 Results

Fig. 13 shows the V_{OC} at the pre-selected photo-current density of 73.3 μA/cm^2, corresponding to an irradiance of 3 W/m^2, calculated from the one-diode model fits of the measured I-V scans (blue circles) and predicted by the new model (orange line). The gray filled area represents the logarithm of the normalized irradiance, which is used as an input to the LTI system predicting the V_{OC}. Fig. 14 shows the measured (blue circles) and the predicted (orange dots) P_{MPP} as well as the P_{MPP} predicted by two static models (green Xs and red plusses), which

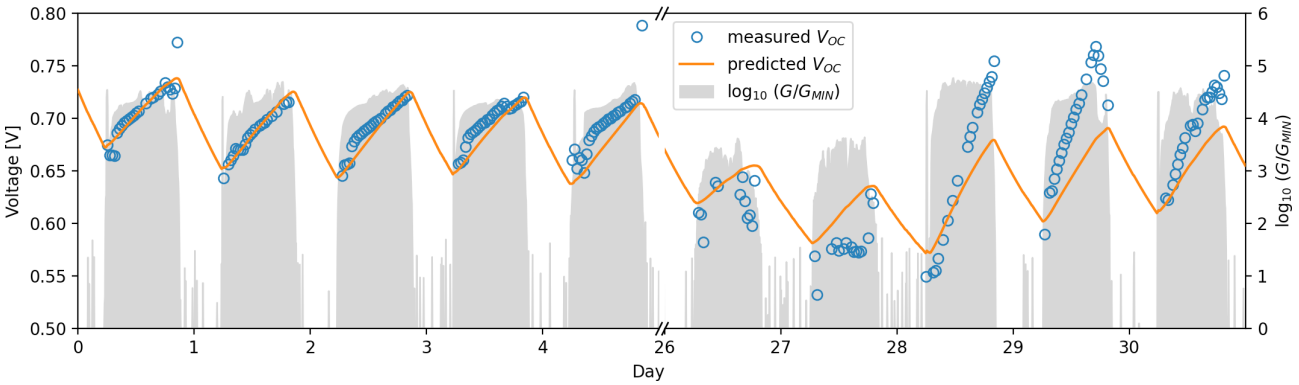

Figure 13: The measured (blue circles) and the predicted (orange line) V_{OC} at the pre-selected photo-current density of 73.3 µA/cm², equivalent to an irradiance of 3 W/m², for the first 5 and last 5 days of August. The gray fill shows the logarithm of the irradiance normalized to the minimum irradiance, which is used as the input to the prediction LTI system.

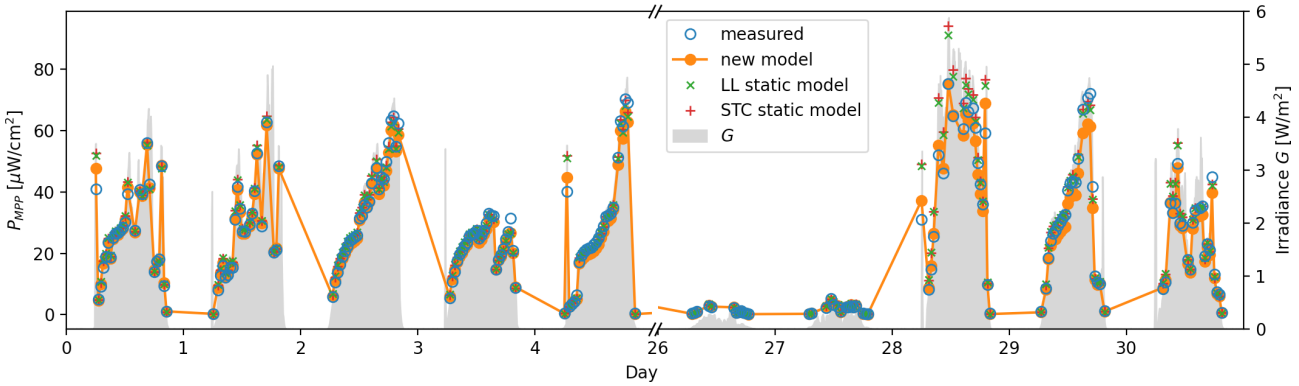

Figure 14: The measured P_{MPP} (blue circles), the P_{MPP} predicted by the new model (orange line with dots), the P_{MPP} predicted using the low-light static model (green Xs), and the P_{MPP} predicted using the STC static model (red plusses) for the first 5 and the last 5 days of August.

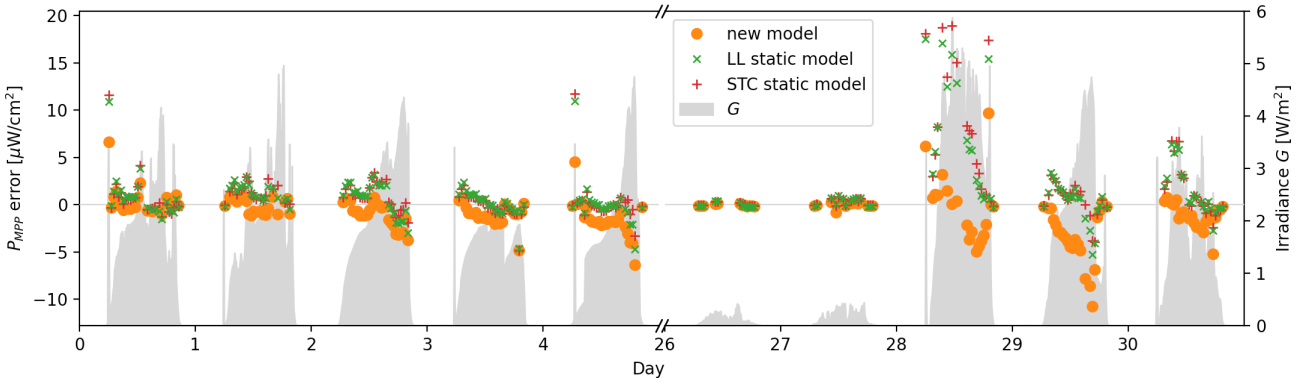

Figure 15: The P_{MPP} prediction errors of the new model (orange dots), the low-light static model (green Xs), and the STC static model (red plusses) for the first 5 and the last 5 days of August.

do not take the LSE into account, to provide a basis for comparison. Fig. 15 shows the errors of the new model (orange dots) and the two reference static models (green Xs and red plusses). The gray fill in Figs. 14 and 15 shows irradiance. All three figures show the data for the first 5 days and the last 5 days of August 2022.

The V_{OC} predicted by the new model follows the measured V_{OC} quite well at the beginning of the month, but not quite as well at the end of the month. The V_{OC} values measured on the 27th and 28th of August (Saturday and Sunday) seem to change quite unpredictably, which is the result of very low irradiance and therefore a low signal to noise ratio. The very low irradiance is consistent

with the blinds being lowered all the way down. Despite this, the predicted V_{OC} values are in the general vicinity of the measured values. On the last three days of August, the model underestimates the LSE and the predicted V_{OC} lags considerably behind the measured V_{OC}. Such discrepancies between the measurements and predictions begin to appear in the second half of the month. This behavior is reflected in the predicted P_{MPP}, which also matches the measured P_{MPP} very well at the beginning of the month, and not nearly as well towards the end of the month.

The static models used as a basis for comparison consist of taking a single *I-V* scan, obtaining a fit to the one-diode model and using the obtained parameters to calculate the P_{MPP} for every point in time based on the irradiance. Energy yield predictions or analysis in outdoor environments are often performed using measured stabilized *I-V* characteristics of the PSC, which means the *I-V* scan is taken only after the cell has been fully light-soaked. Since the fully light-soaked state can be reached quite quickly in a bright outdoor environment, the error introduced by this approach is acceptable in most cases. In the case of low-light environments, however, the LSE may not reach saturation even after an entire day, therefore an *I-V* scan taken sometime in the middle of the day may be more representative. We decided to use both approaches and derive one static model based on an *I-V* scan performed in low-light conditions on the first day of the measurements, when the brightness was the highest (green Xs in figures, hereafter referred to as the low-light or LL static model) and the other based on the *I-V* scan of the fully light-soaked PSC under STC (red plusses in figures, hereafter referred to as the STC static model). The prediction error of the low-light static model is quite well balanced between positive and negative values at the beginning of the month, confirming a good choice of the *I-V* scan to base the model on.

It has to be noted that selecting a different *I-V* scan for the low-light static model can result in either better or worse predictions. EY calculations in particular can easily be manipulated by selecting just the right *I-V* scan to get the desired result on a known dataset. Therefore, EY calculations and their errors are given for completeness and to give an idea of how large errors in the EY can potentially be expected, but are not a reliable measure of the quality of the method. Instead, the mean absolute error (MAE) and root mean square error (RMSE) of the P_{MPP} paint a much clearer picture, although they too depend on the selection of the *I-V* scan in the case of the low-light static model and the selection of the model tuning period in the case of the new model. The STC static model on the other hand is much less tweakable.

A good selection of the tuning period is essential for the performance of the model. Tests showed that the minimum tuning period is 2 days, because this ensures that the relaxation of the LSE is well defined in the training data. Longer training periods are generally beneficial, but not necessarily by much. If the selected training period includes representative conditions, increasing the training period does not improve the model's performance greatly. However, longer tuning periods usually include a wider range of conditions and thus provide a more representative dataset and therefore result in a better performing model.

The P_{MPP} predictions of both static models are very similar and the low-light static model performs only marginally better than the STC static model. However, a closer examination of the predictions shows a considerably different picture. Fig. 16 shows the measured and predicted *J-V* (solid lines) and *P-V* (dotted lines) curves, with the MPP marked with Xs on the *I-V* curves and plusses on the *P-V* curves. The predicted curves of the new model and the low-light static model match the general shape of the measured data very well. The STC static model, on the other hand, predicts a much more gradual drop in current density when approaching V_{OC} and considerably higher V_{OC}, resulting in a lower predicted fill-factor (FF). Although the general shape of the predicted *J-V* curve is a much worse match to the measured data than those of the other models, the combination of increased V_{OC} and decreased FF coincidentally results in almost the same P_{MPP} as in the case of the low-light static model.

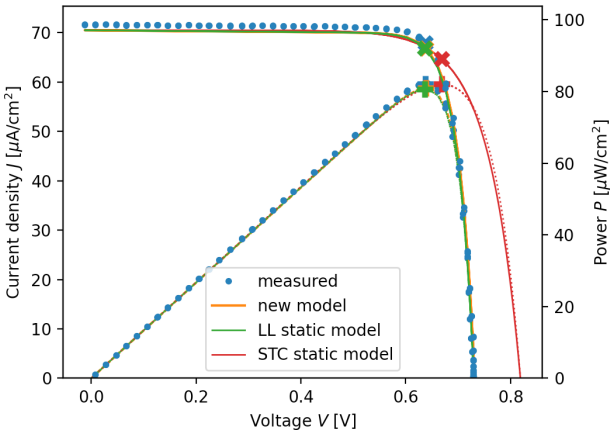

Figure 16: Measured (blue dots) and predicted *J-V* curves (solid lines) and *P-V* curves (dotted lines) of all three prediction models: the new model (orange), the low-light static model (green), and the STC static model (red). The MPP on the *J-V* curve is marked with Xs, and on the *P-V* curve with plusses.

The measured and predicted EY over the course of the month, as well as the MAE and RMSE of all the models

are summarized in Table 2. During the first half of the month the P_{MPP} predictions of the new model mostly outperform the predictions of both static models. However, at the end of the month, the errors of the static models are sometimes lower than those of the new model. Taking the entire prediction period into account, the MAE of the new model is 16.7 % lower than MAE of the low-light static model and 17.1 % lower than MAE of the STC static model. The RMSE indicates slightly lower improvement of 12.3 % and 15.6 % over the low-light and STC static models, respectively. The EY prediction errors of both static models are +6.96 % and +7.76 %, while the EY prediction error of the new model is only -0.72 %, which is extraordinary and probably due to a bit of luck as well.

Table 2: Performance comparison of the new model with the static model.

Parameter	Measure-ment	static model	STC static model	new model
EY [mWh/cm^2]	12.50	13.37	13.47	12.41
EY error [%]	-	+6.96	+7.76	-0.72
MAE(PMPP) [µW/cm^2]*	-	2.21	2.22	1.84
RMSE(PMPP) [µW/cm^2]*	-	3.26	3.39	2.86

* P_{MPP} varies between 0 and 94 µW/cm^2

5 Discussion

The presented model of the LSE in the PSC predicts the state of the PSC based on the history of irradiance quite well in the first half of the month but starts to deviate in the second half. It has to be noted, that the model is never completely reset and errors in prediction accumulate with time. Yet, despite this, the error at the end of the month still remains strictly within ± 13 µW/cm^2 and rarely exceeds ± 5 µW/cm^2 (14 % and 5 % of the observed P_{MPP} range), exhibiting a degree of robustness of the model.

On the other hand, the model cannot predict the small variations the measured V_{OC} exhibits (Fig. 13), even at the beginning of the month. We believe the same basic approach could be used to model those variations as well, but with a more sophisticated LTI system. However, more research is need to isolate individual contributions of external parameters to light-soaking and to more carefully identify the system's response to external stimuli.

The experiment that provided the data for this work was designed to provide data on PSC performance in a realistic, uncontrolled indoor environment and statistical data on such an environment throughout the seasons of the year. As such, it was not optimized to gather data required for the LSE modelling. However, the recorded data was just accurate enough to facilitate the first steps in the LSE modelling in PSCs and inspire further research, which will hopefully provide higher quality data for a more accurate model as well as more reliable and extensive validation. The experiment had several shortcomings if viewed in light of the requirements for LSE research that will have to be improved upon in future research:

- Shading in realistic indoor environments can be very localized, therefore it is very important to place the irradiance sensor as close as possible to the device under test (DUT), or better yet, place several irradiance sensors on opposite sides of the DUT.
- Spectral matching of the irradiance sensor and the PSC remains a challenge for now, especially if the angular sensitivity of both devices needs to match as well. A workaround would be to avoid an uncontrolled environment and strictly control the spectrum of incident light.
- For the purpose of accurate one-diode model fitting, the current measurement accuracy needs to be increased.
- The irradiance within this experiment almost never exceeded 6 W/m^2, therefore the model is only verified within this low irradiance range.

In a more specialized experiment, the influence of temperature could also be characterized and perhaps included in the model. However, within this work, the measured temperature was accounted for only as a parameter of the one-diode model (1), even though it has been established before that it affects the LSE [25] as well. With the very limited changes in temperature in the indoor environment (26.4 °C to 34.0 °C) we assumed that all other sources of uncertainty overshadowed the influence of temperature.

Focusing on the prediction results for the second half of the month, we see several possible reasons for the reduced performance of the model. It is possible that changes in blinds positions (which were not recorded or otherwise logged) changed either the average spectrum of light enough to influence the LSE or changed the shading conditions, which could have led to a smaller indicated irradiance, which could in turn have caused the model to underestimate the LSE. PSCs are also known for their less than optimal long-term stability and it is possible that their performance changed enough during the first month to make a noticeable

difference in how the LSE manifests. However, it is impossible to conclusively determine the cause of the slightly worse performance at the end of the test period from the available data.

6 Conclusions

Within this work a new model for predicting the light-soaking effect (LSE) of perovskite solar cells (PSC) based on the history of their irradiance has been presented. The model uses the current irradiance to calculate the photo-current I_{PH}, the ideality factor n and the shunt resistance R_p of the one-diode model of the PSC. From the irradiance history it calculates the V_{OC} at a preselected current (to isolate the LSE from the influence of the photo-current on the V_{OC}), which is then used to calculate the saturation current of the one-diode model. The thus calculated one-diode model parameters account for the LSE and can be used in further analysis, like P_{MPP} or energy yield calculations.

The proposed model was compared to two static one-diode models over the course of one month and showed a 16.7 % improvement over the low-light static model and 17.1 % improvement over the STC static model in the mean absolute error (MAE) of the P_{MPP} prediction, achieving a MAE of 1.84 µW compared to the 2.21 µW and 2.22 µW of the low-light and STC based static models, respectively, compared to the daily variations of P_{MPP} between 0 and approximately 94 µW.

7 Acknowledgments

I would like to thank M. Topič, M. Jošt, Ž. Ajdič, Š. Tomšič, M. Jankovec and G. Matič for many fruitful discussions. The Research was funded by the Slovenian Research and Innovation Agency, program P2-0415.

8 Conflict of Interest

I have no conflict of interest to declare.

9 References

1. J.-Y. Shao *et al.*, "Recent progress in perovskite solar cells: material science," *Sci. China Chem.*, vol. 66, no. 1, pp. 10–64, Jan. 2023, https://doi.org/10.1007/s11426-022-1445-2.
2. "Best Research-Cell Efficiency Chart Provided by NREL." [Online]. Available: https://www.nrel.gov/pv/assets/pdfs/best-research-cell-efficiencies.pdf. [Accessed: 03-Aug-2023].
3. R. G. Charles, A. Doolin, R. García-Rodríguez, K. Valadez Villalobos, and M. L. Davies, "Circular economy for perovskite solar cells – drivers, progress and challenges," *Energy Environ. Sci.*, 2023, https://doi.org/10.1039/D3EE00841J.
4. A. S. R. Bati, Y. L. Zhong, P. L. Burn, M. K. Nazeeruddin, P. E. Shaw, and M. Batmunkh, "Next-generation applications for integrated perovskite solar cells," *Commun. Mater.*, vol. 4, no. 1, pp. 1–24, Jan. 2023, https://doi.org/10.1038/s43246-022-00325-4.
5. M. Mujahid, C. Chen, W. Hu, Z.-K. Wang, and Y. Duan, "Progress of High-Throughput and Low-Cost Flexible Perovskite Solar Cells," *Sol. RRL*, vol. 4, no. 8, p. 1900556, 2020, https://doi.org/10.1002/solr.201900556.
6. M. Wang *et al.*, "Lead-Free Perovskite Materials for Solar Cells," *Nano-Micro Lett.*, vol. 13, no. 1, p. 62, Jan. 2021, https://doi.org/10.1007/s40820-020-00578-z.
7. X. Liu *et al.*, "Lead-Free Perovskite Solar Cells with Over 10% Efficiency and Size 1 cm2 Enabled by Solvent–Crystallization Regulation in a Two-Step Deposition Method," *ACS Energy Lett.*, vol. 7, no. 1, pp. 425–431, Jan. 2022, https://doi.org/10.1021/acsenergylett.1c02651.
8. A. E. Magdalin *et al.*, "Development of lead-free perovskite solar cells: Opportunities, challenges, and future technologies," *Results Eng.*, vol. 20, p. 101438, Dec. 2023, https://doi.org/10.1016/j.rineng.2023.101438.
9. T. Ahmed Chowdhury, M. A. B. Zafar, M. S.-U. Islam, M. Shahinuzzaman, M. Aminul Islam, and M. Uddin Khandaker, "Stability of perovskite solar cells: issues and prospects," *RSC Adv.*, vol. 13, no. 3, pp. 1787–1810, 2023, https://doi.org/10.1039/D2RA05903G.
10. X. Zhao *et al.*, "Accelerated aging of all-inorganic, interface-stabilized perovskite solar cells," *Science*, vol. 0, no. 0, p. eabn5679, Jun. 2022, https://doi.org/10.1126/science.abn5679.
11. M. Peplow, "A new kind of solar cell is coming: is it the future of green energy?," *Nature*, vol. 623, no. 7989, pp. 902–905, Nov. 2023, https://doi.org/10.1038/d41586-023-03714-y.
12. C.-H. Chen, Z.-K. Wang, and L.-S. Liao, "Perspective on perovskite indoor photovoltaics," *Appl. Phys. Lett.*, vol. 122, no. 13, p. 130501, Mar. 2023, https://doi.org/10.1063/5.0147747.
13. K.-L. Wang, Y.-H. Zhou, Y.-H. Lou, and Z.-K. Wang, "Perovskite indoor photovoltaics: opportunity and challenges," *Chem. Sci.*, vol. 12, no. 36, pp. 11936–11954, 2021, https://doi.org/10.1039/D1SC03251H.

14. T. C.-J. Yang, P. Fiala, Q. Jeangros, and C. Ballif, "High-Bandgap Perovskite Materials for Multijunction Solar Cells," *Joule*, vol. 2, no. 8, pp. 1421–1436, Aug. 2018, https://doi.org/10.1016/j.joule.2018.05.008.
15. Q. Ou *et al.*, "Band structure engineering in metal halide perovskite nanostructures for optoelectronic applications," *Nano Mater. Sci.*, vol. 1, no. 4, pp. 268–287, Dec. 2019, https://doi.org/10.1016/j.nanoms.2019.10.004.
16. E. L. Unger, L. Kegelmann, K. Suchan, D. Sörell, L. Korte, and S. Albrecht, "Roadmap and roadblocks for the band gap tunability of metal halide perovskites," *J. Mater. Chem. A*, vol. 5, no. 23, pp. 11401–11409, Jun. 2017, https://doi.org/10.1039/C7TA00404D.
17. "State of IoT 2023: Number of connected IoT devices growing 16% to 16.7 billion globally," *IoT Analytics*, 24-May-2023. [Online]. Available: https://iot-analytics.com/number-connected-iot-devices/. [Accessed: 08-Nov-2023].
18. Š. Tomšič, M. Jošt, K. Brecl, M. Topič, and B. Lipovšek, "Energy Yield Modeling for Optimization and Analysis of Perovskite-Silicon Tandem Solar Cells Under Realistic Outdoor Conditions," *Adv. Theory Simul.*, vol. 6, no. 4, p. 2200931, 2023, https://doi.org/10.1002/adts.202200931.
19. B. Lipovšek, M. Jošt, Š. Tomšič, and M. Topič, "Energy yield of perovskite solar cells: Influence of location, orientation, and external light management," *Sol. Energy Mater. Sol. Cells*, vol. 234, p. 111421, Jan. 2022, https://doi.org/10.1016/j.solmat.2021.111421.
20. S. Hwang, H. Lee, and Y. Kang, "Energy yield comparison between monofacial photovoltaic modules with monofacial and bifacial cells in a carport," *Energy Rep.*, vol. 9, pp. 3148–3153, Dec. 2023, https://doi.org/10.1016/j.egyr.2023.02.011.
21. I. Haedrich and M. Ernst, "Impact of angular irradiance distributions on coupling gains and energy yield of cell interconnection designs in silicon solar modules in tracking and fixed systems," *J. Phys. Appl. Phys.*, vol. 54, no. 22, p. 224003, Mar. 2021, https://doi.org/10.1088/1361-6463/abe967.
22. M. Jošt *et al.*, "Perovskite Solar Cells go Outdoors: Field Testing and Temperature Effects on Energy Yield," *Adv. Energy Mater.*, vol. 10, no. 25, p. 2000454, 2020, https://doi.org/10.1002/aenm.202000454.
23. M. Remec *et al.*, "From Sunrise to Sunset: Unraveling Metastability in Perovskite Solar Cells by Coupled Outdoor Testing and Energy Yield Modelling," *Adv. Energy Mater.*, vol. n/a, no. n/a, p. 2304452, https://doi.org/10.1002/aenm.202304452.
24. M. Pirc, Ž. Ajdič, D. Uršič, M. Jošt, and M. Topič, "Indoor Energy Harvesting With Perovskite Solar Cells for IoT Applications—A Full Year Monitoring Study," *ACS Appl. Energy Mater.*, vol. 7, no. 2, pp. 565–575, Jan. 2024, https://doi.org/10.1021/acsaem.3c02498.
25. L. Lin *et al.*, "Light Soaking Effects in Perovskite Solar Cells: Mechanism, Impacts, and Elimination," *ACS Appl. Energy Mater.*, Apr. 2023, https://doi.org/10.1021/acsaem.2c04120.
26. B. Li *et al.*, "Revealing the Correlation of Light Soaking Effect with Ion Migration in Perovskite Solar Cells," *Sol. RRL*, vol. 6, no. 7, p. 2200050, 2022, https://doi.org/10.1002/solr.202200050.
27. J. Herterich, M. Unmüssig, G. Loukeris, M. Kohlstädt, and U. Würfel, "Ion Movement Explains Huge VOC Increase despite Almost Unchanged Internal Quasi-Fermi-Level Splitting in Planar Perovskite Solar Cells," *Energy Technol.*, vol. 9, no. 5, p. 2001104, 2021, https://doi.org/10.1002/ente.202001104.
28. B. Cai *et al.*, "Unveiling the light soaking effects of the CsPbI3 perovskite solar cells," *J. Power Sources*, vol. 472, p. 228506, Oct. 2020, https://doi.org/10.1016/j.jpowsour.2020.228506.
29. S. Suckow, T. M. Pletzer, and H. Kurz, "Fast and reliable calculation of the two-diode model without simplifications," *Prog. Photovolt. Res. Appl.*, vol. 22, no. 4, pp. 494–501, 2014, https://doi.org/10.1002/pip.2301.
30. F. Pedregosa *et al.*, "Scikit-learn: Machine Learning in Python," *J. Mach. Learn. Res.*, vol. 12, no. 85, pp. 2825–2830, 2011.

Arrived: 06. 02. 2024
Accepted: 03. 06. 2024